CrossMark

INVITED PAPER

Neutron reflectometry analysis of $Li_4Ti_5O_{12}$/organic electrolyte interfaces: characterization of surface structure changes and lithium intercalation properties

Masaaki Hirayama,[a] Takumi Shibusawa, Ryo Yamaguchi, KyungSu Kim, and Sou Taminato
Department of Chemical Science and Engineering, School of Materials and Chemical Technology, Tokyo Institute of Technology, Midori-ku, Yokohama 226-8502, Japan

Norifumi L. Yamada and Masao Yonemura
Neutron Science Division, Institute of Materials Structure Science, High Energy Accelerator Research Organization (KEK), Tokai, Ibaraki 319-1106, Japan

Kota Suzuki and Ryoji Kanno
Department of Chemical Science and Engineering, School of Materials and Chemical Technology, Tokyo Institute of Technology, Midori-ku, Yokohama 226-8502, Japan

(Received 8 June 2016; accepted 19 August 2016)

The structure changes and lithium intercalation properties in the surface region of $Li_4Ti_5O_{12}$ were investigated using epitaxial $Li_4Ti_5O_{12}$(111) film model electrodes. The discharge–charge measurements, which were conducted with 1 mol/dm^3 $LiPF_6$-containing propylene carbonate, revealed that a 23.8 nm-thick film exhibited a small capacity of 115 mA h/g compared to the theoretical value of 175 mA h/g. In situ neutron reflectometry and ex situ x-ray diffractometry and reflectometry indicated that an irreversible phase change had occurred in the 10-nm surface region of $Li_4Ti_5O_{12}$ during the initial reaction processes. The level of deterioration of the surface structure was significantly reduced by decreasing the $LiPF_6$ concentration; in addition, side reactions of the cell components with the electrolyte species, and their products, may be associated with the deterioration of the $Li_4Ti_5O_{12}$ surface. The surface reactions have a significant impact on the capacity of lithium intercalation in nano-sized $Li_4Ti_5O_{12}$.

I. INTRODUCTION

Lithium ion batteries are driven by electrochemical intercalation, whereby lithium ions are inserted and extracted within gaps in the host lattice without substantial changes to the lattice itself,[1–3] and the performance of lithium ion batteries is intrinsically dependent on the structure and/or composition of the intercalation electrodes.[4–6] $Li_4Ti_5O_{12}$, which possesses a spinel-type structure, has been advocated as an attractive anode material for use in lithium ion batteries of long calendar life. The deintercalation of lithium ions from the $Li_4Ti_5O_{12}$ lattice proceeds with the two-phase coexistence of $Li_4Ti_5O_{12}$ and $Li_7Ti_5O_{12}$ domains with similar lattice parameters,[7–9] which leads to a very small variation in volume during lithium intercalation/deintercalation.[7] The macroscopic zero-strain behavior contributes to the superior cycle stability of the $Li_4Ti_5O_{12}$ electrode during electrochemical cycling.

Nanosizing of $Li_4Ti_5O_{12}$ has recently been the focus for improving the rates of lithium deintercalation by reducing the path lengths for electronic and lithium ion transport in the electrode.[10–13] As the surface area of the $Li_4Ti_5O_{12}$ electrode increases with decreasing particle size, interfacial phenomena at the $Li_4Ti_5O_{12}$/organic liquid electrolyte interface influences the electrode properties.[12,14] Although interfacial behavioral patterns have been widely reported for oxide cathodes and carbon anodes,[15–20] there is insufficient experimental information regarding the $Li_4Ti_5O_{12}$/electrolyte interfaces to fully elucidate the impact of interfacial reactions on the intercalation properties. Some electrolyte species decompose at the $Li_4Ti_5O_{12}$ surface, which results in the formation of a solid electrolyte interphase (SEI) layer,[21–24] and it has been proposed that the composition and electrochemical stability of the SEI layer determines the retention of the discharge–charge capacity of $Li_4Ti_5O_{12}$ electrodes.[21–24] On the electrode side, an irreversible crystal structure change occurs in the surface region of $Li_4Ti_5O_{12}$ during the electrochemical process,[25–27] and these interfacial reactions vary considerably according to the combination of the electrode and the electrolyte materials. These findings suggested the significant

Contributing Editor: Chongmin Wang
[a]Address all correspondence to this author.
e-mail: hirayama@echem.titech.ac.jp
DOI: 10.1557/jmr.2016.320

https://doi.org/10.1557/jmr.2016.320 Published online by Cambridge University Press

 © Materials Research Society 2016

importance of surface phenomena for cycle stability and rate capability of $Li_4Ti_5O_{12}$ anode which is usually operated in the high voltage regions above 1 V versus Li/Li^+. However, previous studies on $Li_4Ti_5O_{12}$/electrolyte interfaces have only focused on one of these combinations, which makes systematic investigation difficult. Furthermore, ex situ experimental techniques such as x-ray photoelectron spectroscopy and transmission electron microscopy were used in most studies, providing interfacial information indirectly.

In this work, we analyzed the interfacial reactions of $Li_4Ti_5O_{12}$ with different electrolytes using an epitaxial-film model electrode and in situ neutron reflectometry (NR). Epitaxial thin films have a single orientation and an atomically small surface roughness of less than a few nanometers, and do not contain addictive carbon or binder,[15,17] which results in an ideal reaction field for investigating interfacial reactions. Furthermore, epitaxial $Li_4Ti_5O_{12}$ films with (111) and (110) orientations have been successfully fabricated on Nb:$SrTiO_3$ single crystal substrates via pulsed laser deposition (PLD).[14,28] NR is a powerful technique that can provide an atomistic understanding of solid/liquid interfaces as a function of the depth,[29] since neutrons have a sufficiently small absorption cross-section for penetrating electrochemical cells so that electrochemical interfaces can be probed. As a light element, lithium has a relatively high neutron scattering power compared to that of x-rays, and the depth profile of the neutron scattering length density (SLD) obtained by curve fitting can reveal the surface structure changes of the $Li_4Ti_5O_{12}$ film during electrochemical processes. Analyses combining in situ NR and ex situ x-ray diffraction (XRD)/x-ray reflectometry (XRR) measurements provided direct information regarding the surface structural changes of $Li_4Ti_5O_{12}$ with different electrolytes, as well as the underlying intercalation properties.

II. EXPERIMENTAL

Epitaxial $Li_4Ti_5O_{12}$(111) thin films were grown on $SrTiO_3$(111) substrates (10 × 10 × 0.5 mm or 20 × 20 × 5 mm, Crystal Base Co., Ltd.) using a KrF excimer laser with a wave length of 248 nm and PLD apparatus (PLAD131, AOV Inc., Tokyo, Japan). The following optimal synthetic conditions were selected based on results of our previous studies[14,28]: oxygen pressure, pO_2 = 6.6 Pa; distance between substrate and target, d = 60 mm; laser frequency, f = 10 Hz; deposition time, t_d = 5–25 min; energy density, E = 0.3–0.4 J/cm^2; temperature, t = 650 °C.

Discharge–charge characteristics were performed using a two-electrode configuration involving two different electrochemical cells: a 2032-type coin-cell and an in situ spectroelectrochemical cell designed for NR.[30] The cells were assembled inside an argon-filled glove box using lithium metal for counter and reference electrodes and the $Li_4Ti_5O_{12}$ thin film as the working electrode. The electrolytes used comprised propylene carbonate (PC; Kishida Chemical Co., Ltd, >99.5%, water content of <30 ppm) and ethylene carbonate–diethyl carbonate with a volume ratio of 3:7 (EC/DEC; Kishida Chemical Co., Ltd., >99.5%, water content of <30 ppm) as the solvents and 0.5, 1.0, or 2.4 mol/dm^3 $LiPF_6$ as the supporting electrolyte. The charge–discharge characteristics were examined at room temperature, and the cut-off voltages were 1.0 and 3.0 V for discharge and charge, respectively. The charge–discharge capacities of the cells were calculated by taking into account the area over which the film was deposited (10 × 8 mm for the coin cells and 15 × 15 mm for the spectroelectrochemical cells), the film thickness and the theoretical density of $Li_4Ti_5O_{12}$ (3.48 g/cm^3).

Ex situ XRD and XRR analyses were performed to investigate the structural changes of $Li_4Ti_5O_{12}$ films induced by electrochemical cycling. The cell was disassembled in the charged state after electrochemical cycling, and the $Li_4Ti_5O_{12}$ film was then washed in dimethyl carbonate. XRD patterns and XRR spectra were collected via an x-ray diffractometer (ATX-G, Rigaku Corporation, Tokyo, Japan) using 0.1541 nm as the x-ray wave length. The thickness, density, and roughness of the films were refined from XRR spectra using the Parratt[31] and MOTOFIT[32] programs, which apply Parratt's method.[33]

In situ NR measurements were performed on SOFIA (BL-16, Materials and Life Science Facility, Japan Proton Accelerator Research Complex, Tokai, Japan), which is a time-of-flight reflectometer.[30,34,35] An electrochemical cell was composed of a $Li_4Ti_5O_{12}/SrTiO_3$ cathode, a Li anode and deuterated carbonate based electrolytes containing $LiPF_6$ as a supporting electrolyte,[30,36] with the purpose of the deuterated electrolytes being to prevent incoherent scattering (80.27 and 2.05 for ^1H and ^2H, respectively). Deintercalation and intercalation were performed via the potentiostatic method using a potentiostat/galvanostat (Ivium Tech., Compactstat, Eindhoven, The Netherlands). The NR spectra were collected using the single-frame mode at 0.3, 0.6, and 1.2°, and the individual data points were combined. The cell conditions were monitored after the cell construction (OCV), at 1.6, 1.4, and 1.2 V (versus Li/Li^+) at the first discharge, 3.0 V at the first charge, and after discharging and charging in the fifth cycle.

III. RESULTS AND DISCUSSION

Figure 1(a) depicts the discharge–charge curves of a 23.8 nm-thick $Li_4Ti_5O_{12}$(111) film, which was synthesized on Nb-doped $SrTiO_3$(111) during the 30 cycles. The spectroelectrochemical cell used for in situ NR consisted of a $Li_4Ti_5O_{12}$(111)/Nb:$SrTiO_3$(111) cathode,

https://doi.org/10.1557/jmr.2016.320 Published online by Cambridge University Press

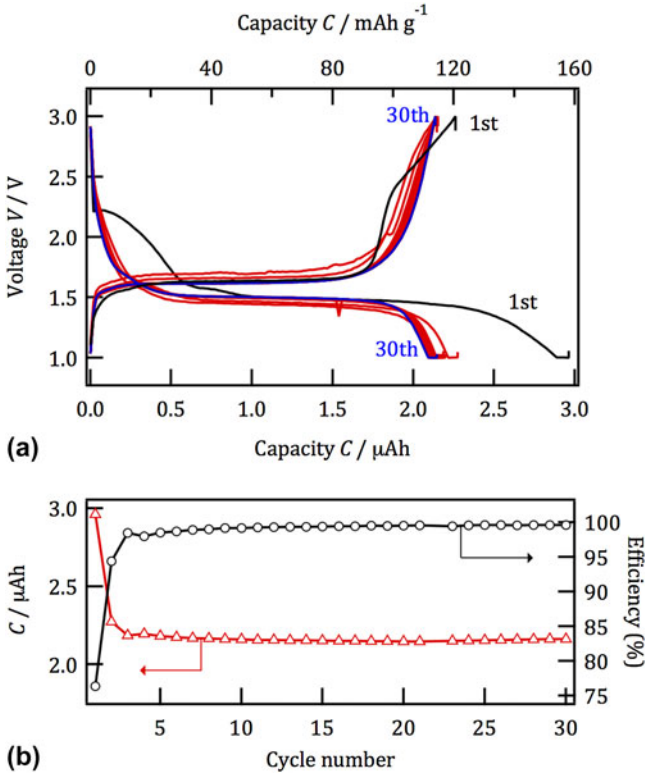


FIG. 1. (a) Discharge–charge curves of a 23.8 nm-thick $Li_4Ti_5O_{12}(111)/SrTiO_3(111)$ film with an electrolyte of 1 mol/dm^3 $LiPF_6$ PC and (b) variation of discharge capacity and cycle efficiency during 30 cycles. The discharge–charge measurements were collected using an in situ NR cell. The constant current applied was approximately 6.6 μA, which corresponds to a current density of 350 mA/g (2 C) for the $Li_4Ti_5O_{12}$ film electrode. The active area of the $Li_4Ti_5O_{12}(111)$ film was 15 × 15 mm.

1.0 mol/dm^3 $LiPF_6$-containing PC electrolyte, and a Li metal anode. A plateau region was observed at around 1.5 and 1.6 V in the discharge and charge curves, respectively, which represents a two-phase coexistence of spinel-type $Li_{4+\alpha}Ti_5O_{12}$ and ordered rock-salt type $Li_{7-\beta}Ti_5O_{12}$ domains[12,13,37] that demonstrates the lithium intercalation activity of the $Li_4Ti_5O_{12}(111)$ film electrode. The first discharge and charge curves showed slope regions from 2.3 to 1.7 V and from 2.4 to 3.0 V, respectively, which could be associated with side reactions occurring in the cell. As a Nb:$SrTiO_3(111)$/1.0 mol/dm^3 $LiPF_6$ PC/Li cell delivered no significant capacities in these voltage regions (see Supporting Information S1), electrochemical decomposition of electrolyte species did not contribute the discharge and charge capacities in the slope regions. Thus, the slope regions observed during the first cycle suggested an irreversible phase change in the $Li_4Ti_5O_{12}(111)$ film. During the following cycles, the $Li_4Ti_5O_{12}(111)$ film exhibited reversible lithium intercalation with high capacity retention and high cycle efficiency, as shown in Fig. 1(b). The discharge capacity was 2.18 μAh (116 mA h/g) at the 3rd cycle and remained stable at 2.16 μAh (115 mA h/g) at the 30th cycle. The discharge capacities were much smaller than the theoretical value of lithium intercalation from $Li_4Ti_5O_{12}$ to $Li_7Ti_5O_{12}$ of 3.28 μAh for the 23.8 nm-thick film (corresponding to 175 mA h/g). From these results, we can speculate that lithium intercalation reversibly proceeded into the $Li_4Ti_5O_{12}(111)$ except for a part of the film which irreversibly changed to an inactive phase at the initial electrochemical process.

Ex situ XRD and XRR analyses were conducted to investigate the structural change of the $Li_4Ti_5O_{12}(111)$ induced by the electrochemical processes. Figure 2(a) shows out-of-plane XRD patterns of the 23.8 nm-thick $Li_4Ti_5O_{12}(111)$ in pristine condition and after 30 cycles. The intensities were normalized using the value of the $SrTiO_3(111)$ diffraction peak, which was obtained by fitting a Gaussian curve. The pristine film generated diffraction peaks at 18.4°, 37.2°, and 79.6° along the out-of-plane [111] direction, which are attributed to the *hhh* diffraction peaks of $Li_4Ti_5O_{12}$ with the $Fd\bar{3}m$ space group, and these observations confirmed the (111) orientation of the $Li_4Ti_5O_{12}$ film. The out-of-plane lattice parameter was calculated to be 8.365(3) Å, and no considerable change in lattice parameter was observed for the cycled sample, which supported the reversible intercalation of the $Li_4Ti_5O_{12}$ film during the 30 cycles. By contrast, the diffraction peaks showed a decrease in the intensities after the electrochemical cycling, which indicates a partial phase change from $Li_4Ti_5O_{12}$ to another phase, as proposed from transmission electron microscopy and scanning probe microscopy studies.[26,27] Figure 2(b) illustrates the XRR analysis results and the x-ray SLD profiles of the pristine and cycled $Li_4Ti_5O_{12}$ films. The reflectivity spectra were plotted as functions of the scattering vector, $Q_z = 4\pi \sin\theta/\lambda$, where λ is the x-ray wave length (0.1541 nm) and θ is the glancing angle. A two-layer model consisting of a surface impurity and the $Li_4Ti_5O_{12}$ film closely fitted the reflectivity curve of the pristine film. The thickness, surface roughness, and x-ray SLD value of the $Li_4Ti_5O_{12}$ film were refined to 23.6 ± 0.4 nm, 1.5 ± 0.6 nm, and 2.83 ± 0.02 × 10^{-3} nm^{-2}, respectively [Fig. 2(c)]. The SLD value was consistent with that expected for stoichiometric $Li_4Ti_5O_{12}$ (2.82 × 10^{-3} nm^{-2}). The pristine film was covered with a surface impurity layer with a thickness of 1.0 ± 0.3 nm, and the surface impurity had a SLD value of 1.69 ± 0.04 × 10^{-3} nm^{-2}. Considering the SLD values of typical lithium containing oxides (1.74 × 10^{-2} nm^{-2} for Li_2CO_3, 1.61 × 10^{-3} nm^{-2} for Li_2O, and 1.25 × 10^{-3} nm^{-2} for LiOH), the surface layer appears to mainly consist of Li_2CO_3. The fringes of the XRR spectrum of the cycled sample shifted to lower Q_z values, which indicates an increase in the total thickness of the film [Fig. 2(b)]. Thus, we added a SEI layer to the structural model since a SEI layer has been reported to form on the $Li_4Ti_5O_{12}$

https://doi.org/10.1557/jmr.2016.320 Published online by Cambridge University Press

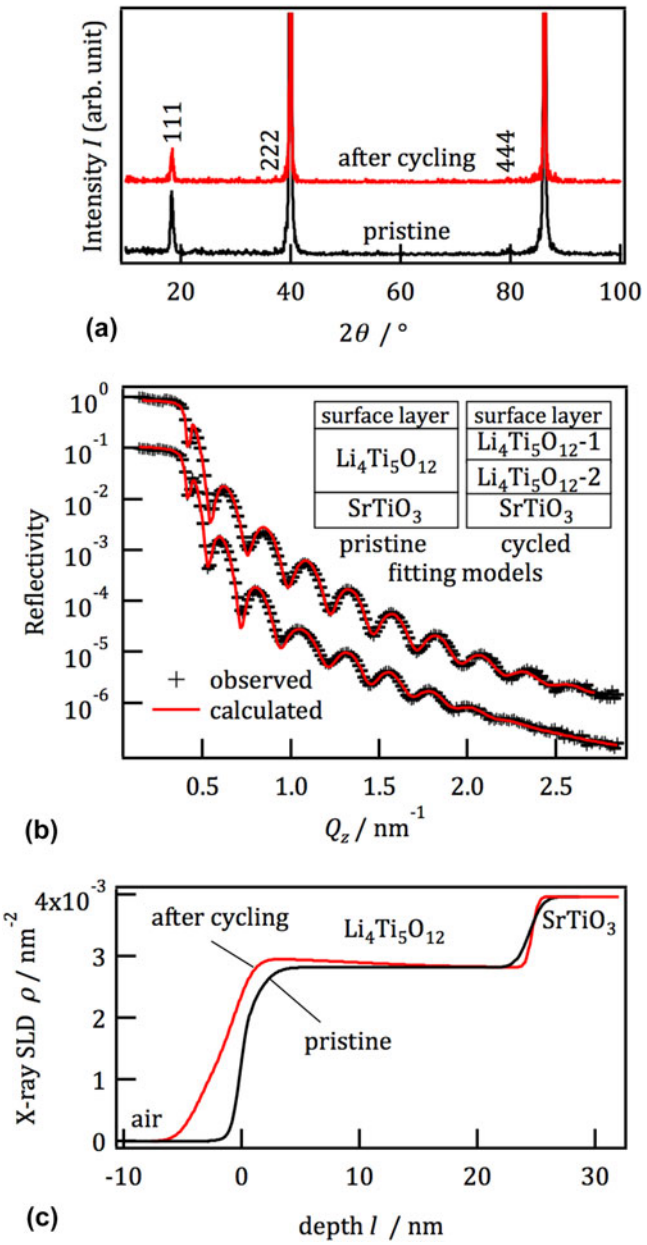


FIG. 2. (a) Out-of-plane XRD patterns, (b) XRR analysis results of $Li_4Ti_5O_{12}(111)/SrTiO_3(111)$ films, and (c) x-ray SLD profiles in pristine condition and following electrochemical cycling. The XRD patterns and XRR spectra were collected in air.

surface by electrolyte decomposition.[21–24] Furthermore, we divided the $Li_4Ti_5O_{12}$ layer into two parts: a bulk region and a surface region for investigating the irreversible phase change indicated by the discharge–charge and XRD results. The three-layer model composed of SEI layer/$Li_4Ti_5O_{12}$-surface/$Li_4Ti_5O_{12}$-bulk/$SrTiO_3$ fitted more closely ($\chi^2 = 5.22 \times 10^{-3}$) than the three-layer model composed of SEI layer/$Li_4Ti_5O_{12}$/$SrTiO_3$ ($\chi^2 = 6.41 \times 10^{-3}$). The fitting curve and the SLD profile as calculated using the four-layer model are shown in Figs. 2(b) and 2(c). In the SLD profile, the bulk region of the cycled $Li_4Ti_5O_{12}$ had a similar SLD value to that of the pristine sample, whilst the 10-nm surface region had a higher SLD value of $3.00 \pm 0.03 \times 10^{-3}$ nm^{-2}. The XRR analyses highlighted the phase change in a high-density phase in the surface region. The SEI layer on the $Li_4Ti_5O_{12}$ surface had a thickness of approximately 4 nm after 30 cycles, and the slope of the SLD profile implied a gradation of chemical composition in the SEI layer.

To clarify the phase change process occurring at the $Li_4Ti_5O_{12}$ surface, we conducted in situ NR analyses at the $Li_4Ti_5O_{12}$/$LiPF_6$-containing PC interface upon battery operation. Figure 3 shows the NR spectrum fitting results and neutron SLD profiles of the $Li_4Ti_5O_{12}(111)$ film during the first and fifth discharge–charge processes. The reflectivity spectra were plotted as functions of the scattering vector, $Q_z = 4\pi \sin\theta/\lambda$, where λ is the neutron wave length and θ is the glancing angle. Similar to the XRR analysis, a two-layer model consisting of surface impurity/$Li_4Ti_5O_{12}$/$SrTiO_3$ fitted closely with the reflectivity curve for the pristine film [Fig. 3(a)]. The SLD value of the pristine $Li_4Ti_5O_{12}$ films was $2.03 \pm 0.04 \times 10^{-4}$ nm^{-2}, which is consistent with the theoretical value of 2.04×10^{-4} nm^{-2} as calculated with the ICSD data (#15787). The pristine film was covered with a surface impurity layer with a thickness of 2.0 ± 0.3 nm, and the surface impurity had a higher neutron SLD value than the $Li_4Ti_5O_{12}$ layer [Fig. 3(b)]. Considering the SLD values of typical lithium containing oxides (3.46×10^{-4} nm^{-2} for Li_2CO_3, 8.15×10^{-5} nm^{-2} for Li_2O, and 6.02×10^{-6} nm^{-2} for LiOH), the surface layer consisted of Li_2CO_3, which is consistent with the XRR result. The formation of the carbonate and hydroxide components was indicated by x-ray photoelectron spectroscopy (see Supporting Information S2). These observations demonstrate that NR can detect the structural changes that occur within several nanometers of the electrode surface.

NR spectra collected under the electrochemical conditions were analyzed using a three-layer model ($SrTiO_3$/$Li_4Ti_5O_{12}$-bulk/$Li_4Ti_5O_{12}$-surface/surface impurity or SEI/electrolyte), which was a simple extension of the model used for the cycled sample in the ex situ XRR analysis. Following the cell construction (OCV: open circuit voltage), the SLD value of the $Li_4Ti_5O_{12}$ layer increased in the 10–15 nm region from the $Li_4Ti_5O_{12}$/electrolyte interface [Fig. 3(b)], whereas no significant change was observed in the bulk region. This result indicates that the phase change from the $Li_4Ti_5O_{12}$ was initiated following soaking in the electrolyte prior to electrochemical cycling. Kitta et al. have reported that a phase transition to a lithium-deficient rocksalt ($LiTi_5O_{10.5}$) occurs at the $Li_4Ti_5O_{12}$ surface in 1.0 mol/dm^3 $LiPF_6$-containing PC electrolyte, characterized from TEM/electron energy-loss spectroscopy.[26]

https://doi.org/10.1557/jmr.2016.320 Published online by Cambridge University Press

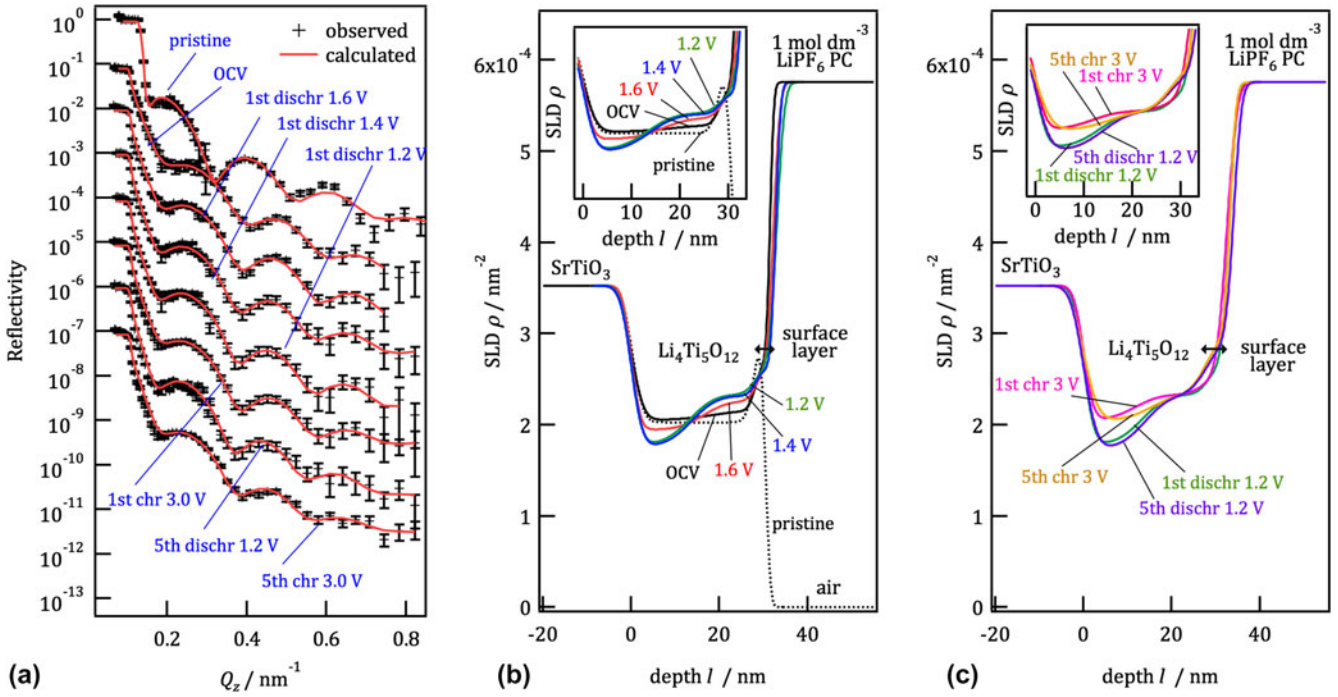


FIG. 3. (a) In situ NR analysis results of epitaxial $Li_4Ti_5O_{12}$(111) films during cycles 1 and 5 in 1 mol/dm^3 $LiPF_6$ PC electrolyte. Refined neutron SLD profiles (b) at the first discharge and (c) during the following processes. The insets in (b, c) depict magnified profiles near the $Li_4Ti_5O_{12}$ regions.

The SLD increase in the surface region is consistent with the previous report, because the lithium-deficient phase should have a higher SLD value than $Li_4Ti_5O_{12}$ because natural lithium has a negative coherent scattering length for neutrons (-1.9 fm for ^{7}Li:^{6}Li = 92.5:7.5). Further, the decrease in the SLD value of the surface impurity region under the OCV condition was observed, which indicates the chemical or electrochemical reactions of the surface impurity phases with electrolyte species at the interface. This could be attributed to the initiation process of the SEI formation. During the first discharge from OCV to 1.2 V, the $Li_4Ti_5O_{12}$ surface region showed a further increase in the SLD, and the phase change proceeded in the surface region during the first discharge. In contrast to the surface region, the bulk region showed no significant change in the SLD from the OCV to 1.6 V and from 1.4 V to 1.2 V. Thus, the discharge capacity observed from 3.0 V to 1.6 and 1.4 V–1.0 V in the first discharge curve may primarily correspond to the phase change of $Li_4Ti_5O_{12}$ in the surface region. The SLD value in the $Li_4Ti_5O_{12}$ bulk region decreased to $1.76 \pm 0.08 \times 10^{-4}$ nm^{-2} from 1.6 V to 1.4 V. The decrease in the SLD corresponds to lithium intercalation in the $Li_4Ti_5O_{12}$ bulk region, which was consistent with the plateau region observed at around 1.5 V in the first discharge curve. The SLD value of the bulk region at the discharged state corresponded to the theoretical value for $Li_7Ti_5O_{12}$ (1.71×10^{-4} nm^{-2}). The lithium intercalation proceeded in the $Li_4Ti_5O_{12}$ bulk region through the surface region. The neutron SLD profiles during the subsequent conditions are shown in Fig. 3(c). After the first charging, the SLD value in the $Li_4Ti_5O_{12}$ bulk reversibly increased to 2.02×10^{-4} nm^{-2}, and the $Li_4Ti_5O_{12}$ bulk showed similar SLD values under the discharged and charged conditions at cycle 5 to those observed at the first cycle. Furthermore, the SLD value and the thickness of the $Li_4Ti_5O_{12}$ surface region remained stable at around 2.3×10^{-4} nm^{-2} and 15 nm after the first cycle, respectively. The low electrochemical activity of the surface-reconstructed phase may cause a decrease in the reversible capacity, which is consistent with the small discharge–charge capacities of the $Li_4Ti_5O_{12}$(111) film (approximately 115 mA h/g) compared to the theoretical value (175 mA h/g). In contrast, highly-reversible lithium intercalation proceeds in the bulk region by lithium diffusion through the surface region during the electrochemical cycling. The SEI layer at the interface was grown in the initial cycles, and the thickness after the fifth cycle was 6.1 ± 0.2 nm. The SEI formation could suppress the further phase change in the surface region of $Li_4Ti_5O_{12}$. The depth profiling of the $Li_4Ti_5O_{12}$/electrolyte interface using in situ NR clarified the intermediate process of the surface-reconstruction and the SEI formation during the initial electrochemical cycling.

To investigate the effect of the electrolyte composition on the surface-reconstruction behavior, we conducted NR analyses of the $Li_4Ti_5O_{12}$(111) film in contact with different electrolytes. Figure 4 shows NR analysis results of $Li_4Ti_5O_{12}$(111) films in pristine condition and following

https://doi.org/10.1557/jmr.2016.320 Published online by Cambridge University Press

soaking in different electrolytes of 2.4 mol/dm^3 $LiPF_6$ PC and 1.0 mol/dm^3 $LiPF_6$ EC/DEC (3:7 vol.). Both pristine $Li_4Ti_5O_{12}$(111) films were covered with the surface impurity layer. NR spectra collected under the OCV condition were analyzed using the three-layer model ($SrTiO_3$/$Li_4Ti_5O_{12}$-bulk/$Li_4Ti_5O_{12}$-surface/SEI/electrolyte) [Figs. 4(a) and 4(b)], which was the same model used for the $Li_4Ti_5O_{12}$(111) film in the 1.0 mol/dm^3 $LiPF_6$ PC electrolyte. When the film electrode was soaked in the 2.4 mol/dm^3 $LiPF_6$ PC electrolyte, the SLD increased in the entire region of the 16 nm-thick $Li_4Ti_5O_{12}$ film [Fig. 4(c)] and the SLD value of approximately 2.4×10^{-4} nm^{-2} was similar to that observed for the $Li_4Ti_5O_{12}$ surface following the first cycle in the 1.0 mol/dm^3 $LiPF_6$ PC (2.5×10^{-4} nm^{-2}). The surface-reconstruction could be promoted via contact with the PC electrolyte of higher $LiPF_6$ content. Conversely, the $Li_4Ti_5O_{12}$ layer showed no significant changes in the SLD using 1.0 mol/dm^3 $LiPF_6$ EC/DEC electrolyte [Fig. 4(d)]. Furthermore, no surface-reconstruction proceeded at the $Li_4Ti_5O_{12}$ surface following soaking in the EC/DEC-based electrolyte, and the surface-reconstruction of $Li_4Ti_5O_{12}$ was influenced by the solvent and the solute species in the organic electrolytes.

Figure 5 shows the discharge–charge curves of the coin-type cell, which consisted of a 23.5 nm-thick $Li_4Ti_5O_{12}$(111) cathode, 1 mol/dm^3 $LiPF_6$ PC electrolyte, and a Li anode. The discharge–charge curves had no clear plateau region at around 1.5 V, which corresponds to the lithium intercalation even though the same combination of cathode, electrolyte, and anode materials were used. It is generally considered that water and hydrogen fluoride in electrolytes lead to electrode deterioration, but it could not explain the difference in the deterioration because the coin-type cell contained a smaller amount of the electrolyte (~0.5 mL) than the in situ spectroelectrochemical cell (~5 mL). In contrast to the in situ spectroelectrochemical cell, which was made from electronically-insulating poly-chloro-trifluoro-ethylene, the coin-type cell was made from electron-conductive stainless steel. Thus, side reactions of the cell body with the electrolyte species could not have been negligible to identify the intercalation properties of the $Li_4Ti_5O_{12}$(111) film. The side reactions were investigated via the discharge–charge curves of the Nb:$SrTiO_3$ substrate in the 1 mol/dm^3 $LiPF_6$ PC electrolyte which were collected using the coin-type cell [Fig. S1(b)]. The Nb:$SrTiO_3$ substrate without the deposited $Li_4Ti_5O_{12}$ active material exhibited the first discharge and discharge capacities of 1.6 and 1.2 μAh, respectively. These values were much larger than those

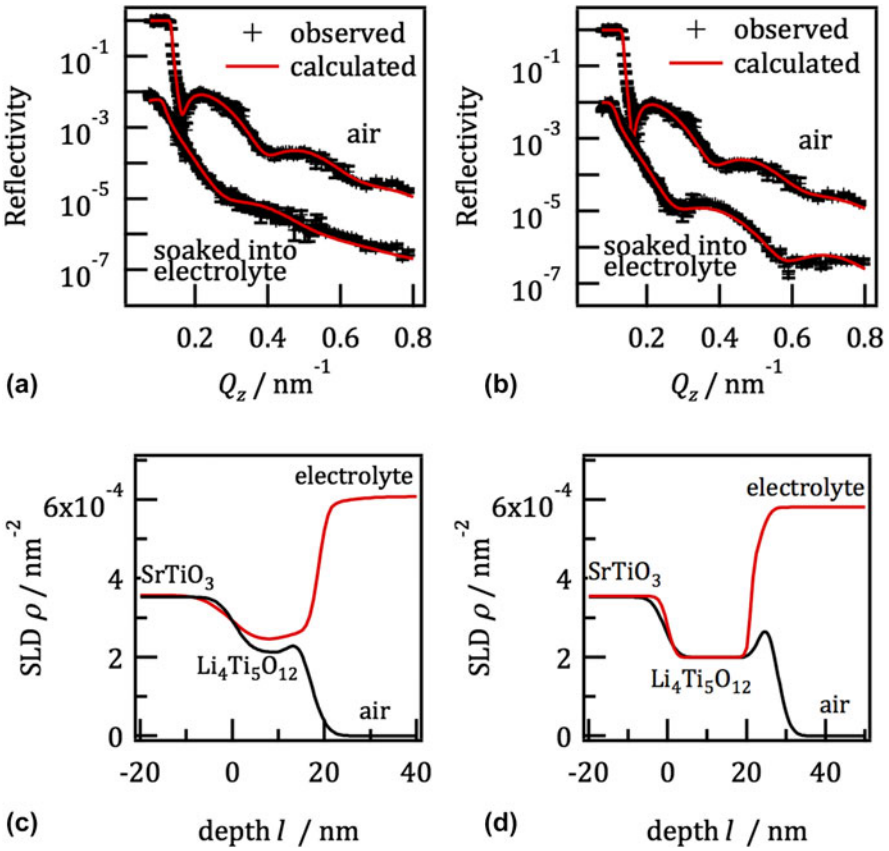


FIG. 4. (a, b) In situ reflectometry analysis results and (c, d) neutron SLD profiles of epitaxial $Li_4Ti_5O_{12}$(111) films in pristine conditions and after soaking in different electrolytes of 2.4 mol/dm^3 $LiPF_6$ PC (a, c) and 1 mol/dm^3 $LiPF_6$ EC:DEC (3:7 vol.) (b, d).

https://doi.org/10.1557/jmr.2016.320 Published online by Cambridge University Press

observed for the in situ spectroelectrochemical cell [Fig. S1(a)], which confirmed the significance of the side reactions in the coin-type cell.

To further understand the effects of the side reactions on the intercalation inactivity of the $Li_4Ti_5O_{12}(111)$ film, the discharge–charge measurements were conducted using coin-type cells with different electrolytes. Figure 6 shows the discharge–charge curves of 10-nm-thick $Li_4Ti_5O_{12}(111)$ films in PC and EC/DEC based electrolytes with different $LiPF_6$ concentrations. The insets in each figure depict the dQ/dV plots at the first and 50th cycles. The discharge–charge curves of all coin-type cells mainly consisted of the slope regions, which were associated with the side reactions, and the capacities of the slope regions increased as the $LiPF_6$ concentration increased, which indicated the participation of the Li^+ and PF_6^- ions in the side reactions. When the 0.5 mol/dm^3 $LiPF_6$-containing PC was used as the electrolyte, the plateau regions were observed at around 1.4 and 1.7 V in the discharge and charge curves, respectively [Fig. 6(a)]. The sharp dQ/dV peaks observed at the 50th cycle confirmed that the reversible lithium intercalation proceeded in the $Li_4Ti_5O_{12}(111)$ film. By contrast, the dQ/dV peaks became smaller as the $LiPF_6$ concentration increased to 1.0 and 2.4 mol/dm^3 [Figs. 6(b) and 6(c)]. As described in the above sections, the $Li_4Ti_5O_{12}(111)$ film delivered the reversible lithium intercalation using the spectroelectrochemical cell, even when the 1.0 mol/dm^3 $LiPF_6$-containing PC electrolyte was used. Thus, we can speculate that the side reactions between coin-cell components and the electrolyte species generate some products that enhance the deterioration of the $Li_4Ti_5O_{12}$ electrode. It must be noted that the $Li_4Ti_5O_{12}(111)$ films in $LiPF_6$-containing EC/DEC electrolytes showed clear plateau regions in the discharge–charge curves as the $LiPF_6$ concentration increased from 0.5 to 2.4 mol/dm^3

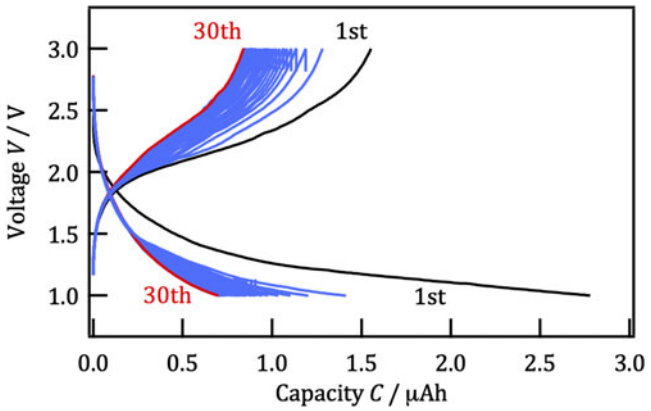


FIG. 5. Discharge–charge curves of a 23.5 nm-thick $Li_4Ti_5O_{12}(111)/SrTiO_3(111)$ film with an electrolyte of 1 mol/dm^3 $LiPF_6$ PC. The discharge–charge measurements were collected using a 2032-type coin-cell. The constant current applied was approximately 1.3 μA, which corresponds to a current density of 175 mA/g (1 C) for $Li_4Ti_5O_{12}$ film electrode. The active area of the $Li_4Ti_5O_{12}(111)$ film was 10 × 8 mm.

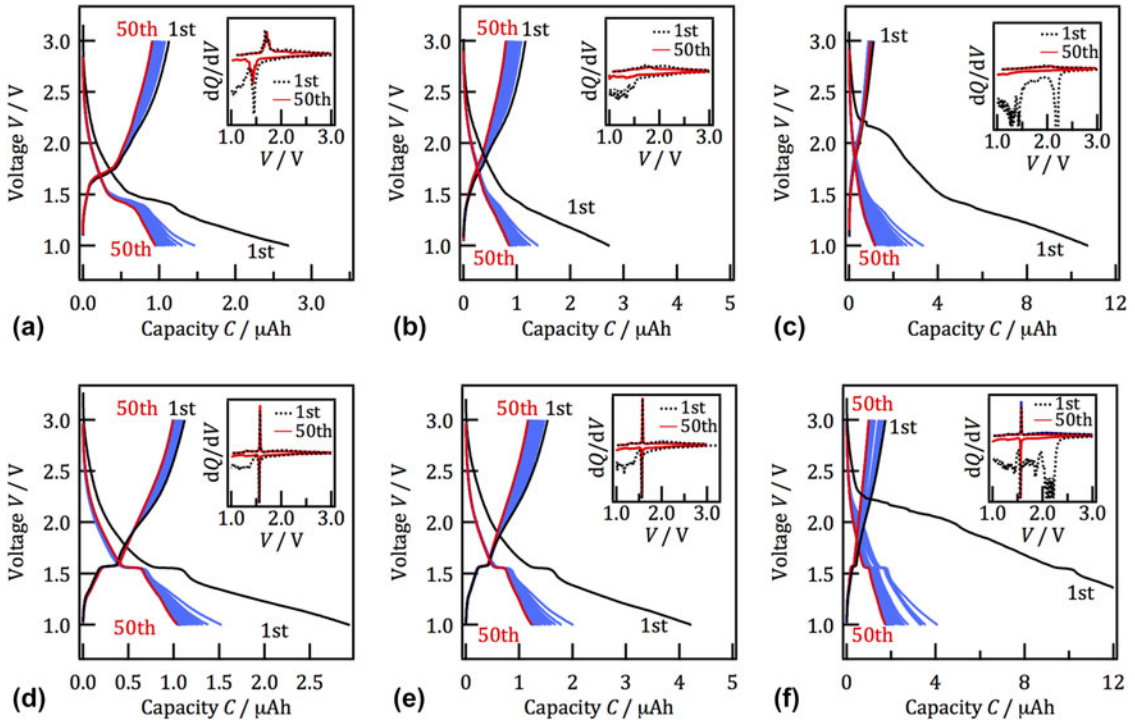


FIG. 6. Discharge–charge curves of 10-nm-thick $Li_4Ti_5O_{12}(111)/SrTiO_3(111)$ films with (a–c) PC and (d–f) EC/DEC(3:7 vol.) electrolytes containing (a, d) 0.5, (b, e) 1.0 and (c, f) 2.4 mol/dm^3 $LiPF_6$. The constant current applied was approximately 0.5 μA, which corresponds to a current density of 175 mA/g (1 C) for $Li_4Ti_5O_{12}$ film electrode.

https://doi.org/10.1557/jmr.2016.320 Published online by Cambridge University Press

[Figs. 6(d)–6(e)]. The discharge capacities in the plateau regions at the 50th cycle were 0.17, 0.19, and 0.18 μAh when the $LiPF_6$ concentrations were 0.5, 1.0, and 2.4 mol/dm^3, respectively, which indicates no dependence of the capacity on the $LiPF_6$ concentration. Furthermore, the dQ/dV peaks were observed at around 1.55 V for both discharge and charge processes, showing a considerably small polarization compared to those observed for the PC-based electrolytes. These results confirmed that the highly-reversible lithium intercalation of $Li_4Ti_5O_{12}$ proceeded in the $LiPF_6$-containing EC/DEC electrolytes. Figure 7 shows XRD patterns of the 10-nm-thick $Li_4Ti_5O_{12}$(111) films after 50 cycles in different electrolytes. The $Li_4Ti_5O_{12}$(111) film cycled in the 1.0 mol/dm^3 $LiPF_6$ EC/DEC showed a 111 diffraction peak at 18.5°, which supports the reversible lithium intercalation. By contrast, the $Li_4Ti_5O_{12}$(111) films cycled in the $LiPF_6$ PC electrolytes showed a diffraction peak at 22.5°, which could not be attributed to the $Li_4Ti_5O_{12}$ and $Li_7Ti_5O_{12}$ spinels. An irreversible phase change from the spinel-type phase was clearly detected after the discharge–charge reactions in the coin-type cells. The intensity ratios of the $Li_4Ti_5O_{12}$(111) to the new peaks decreased with $LiPF_6$ concentration, and the $Li_4Ti_5O_{12}$(111) peak was not observed for the sample cycled in the 2.4 mol/dm^3 $LiPF_6$ PC. The decrease in the intensity ratio can be reasonably related to the decrease in the electrochemical capacity in the plateau regions shown as Figs. 6(a)–6(c). Our results demonstrated that the electrochemical stability of the surface region of $Li_4Ti_5O_{12}$ varied with electrolyte composition and cell components, and a phase change from the $Li_4Ti_5O_{12}$ spinel to an electrochemically-inactive phase occurs during the initial electrochemical process, which results in the small capacity and large polarization during the subsequent cycles.

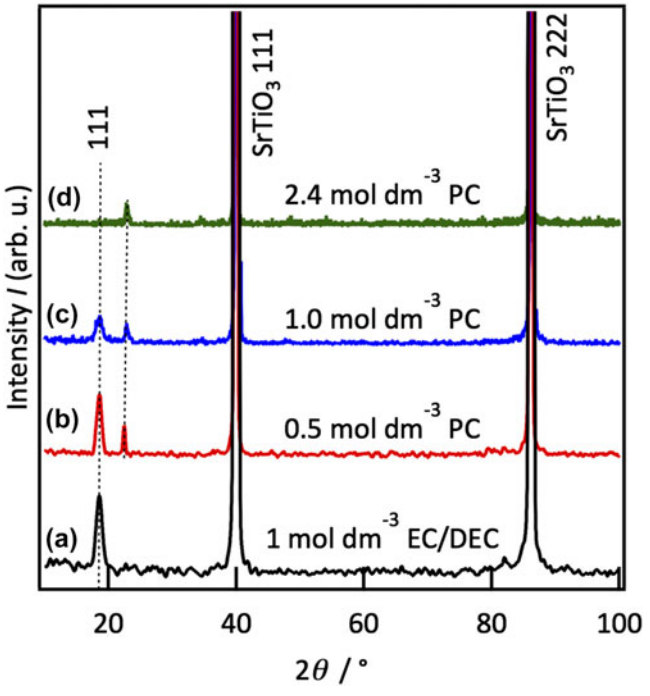


FIG. 7. Ex situ XRD patterns of the 10-nm-thick $Li_4Ti_5O_{12}$(111) films following 50 cycles in (a) 1 mol/dm^3 $LiPF_6$ EC:DEC (3:7 vol.) and (b) 0.5, (c) 1.0, and (d) 2.4 mol/dm^3 $LiPF_6$ PC electrolytes.

IV. CONCLUSION

The surface structure changes and lithium intercalation properties of the $Li_4Ti_5O_{12}$ anode have been investigated using epitaxial-film model electrodes and x-ray and neutron scattering techniques. The NR analyses revealed that the phase change occurs in the 10-nm surface region from the $Li_4Ti_5O_{12}$/organic electrolyte interfaces during the initial reaction processes. The surface-reconstructed phase formed in the $LiPF_6$-containing PC electrolytes limits the lithium intercalation although the surface-reconstruction behavior is highly influenced by the electrolyte composition and the cell component. The $Li_4Ti_5O_{12}$ surface does not show transitions to the low-active phase in the EC/DEC based electrolytes, which leads to highly-reversible lithium intercalation. The coin-type cells lead to further side reactions of electrolyte species, and the products could be associated with electrode deterioration at the $Li_4Ti_5O_{12}$ surface. Our results have demonstrated the importance of surface reactions in the development of $Li_4Ti_5O_{12}$ anodes for lithium ion batteries of high power density.

ACKNOWLEDGMENTS

This work was partly supported by a Grant-in-Aid for Scientific Research (A, C) of Japan Society for the Promotion of Science (Nos. 25410237, 25248051, and 16K05929). The neutron experiments were performed as projects approved by the Japan Proton Accelerator Research Complex (2010A0057, 2013B0166, 2015A0233).

REFERENCES

1. M. Mohri, N. Yanagisawa, Y. Tajima, H. Tanaka, T. Mitate, S. Nakajima, M. Yoshida, Y. Yoshimoto, T. Suzuki, and H. Wada: Rechargeable lithium battery based on pyrolytic carbon as a negative electrode. *J. Power Sources* **26**, 545 (1989).
2. R. Kanno, Y. Takeda, T. Ichikawa, K. Nakanishi, and O. Yamamoto: Carbon as negative electrodes in lithium secondary cells. *J. Power Sources* **26**, 535 (1989).
3. K. Mizushima, P.C. Jones, P.J. Wiseman, and J.B. Goodenough: Li_xCoO_2 ($0 < x < 1$): A new cathode material for batteries of high energy density. *Mater. Res. Bull.* **15**, 783 (1980).
4. L. Croguennec, C. Pouillerie, A.N. Mansour, and C. Delmas: Structural characterisation of the highly deintercalated $Li_xNi_{1.02}O_2$ phases (with $x \leq 0.30$). *J. Mater. Chem.* **11**, 131 (2001).
5. M.M. Thackeray: Manganese oxides for lithium batteries. *Prog. Solid State Chem.* **25**, 1 (1997).
6. M.M. Thackeray, W.I.F. David, P.G. Bruce, and J.B. Goodenough: Lithium insertion into manganese spinels. *Mater. Res. Bull.* **18**, 461 (1983).

https://doi.org/10.1557/jmr.2016.320 Published online by Cambridge University Press

7. F. Ronci, P. Reale, B. Scrosati, S. Panero, V. Rossi Albertini, P. Perfetti, M. di Michiel, and J.M. Merino: High-resolution in-situ structural measurements of the $Li_{4/3}Ti_{5/3}O_4$ "Zero-Strain" insertion material. *J. Phys. Chem. B* **106**, 3082 (2002).
8. S. Panero, P. Reale, F. Ronci, B. Scrosati, P. Perfetti, and V. Rossi Albertini: Refined, in-situ EDXD structural analysis of the $Li[Li_{1/3}Ti_{5/3}]O_4$ electrode under lithium insertion-extraction. *Phys. Chem. Chem. Phys.* **3**, 845 (2001).
9. S. Scharner, W. Weppner, and P. Schmid-Beurmann: Evidence of two-phase formation upon lithium insertion into the $Li_{1.33}Ti_{1.67}O_4$ spinel. *J. Electrochem. Soc.* **146**, 857 (1999).
10. Y. Wang, H. Liu, K. Wang, H. Eiji, Y. Wang, and H. Zhou: Synthesis and electrochemical performance of nano-sized $Li_4Ti_5O_{12}$ with double surface modification of Ti(III) and carbon. *J. Mater. Chem.* **19**, 6789 (2009).
11. A. Jaiswal, C.R. Horne, O. Chang, W. Zhang, W. Kong, E. Wang, T. Chern, and M.M. Doeff: Nanoscale $LiFePO_4$ and $Li_4Ti_5O_{12}$ for high rate Li-Ion batteries. *J. Electrochem. Soc.* **156**, A1041 (2009).
12. W.J.H. Borghols, M. Wagemaker, U. Lafont, E.M. Kelder, and F.M. Mulder: Size effects in the $Li_{4+x}Ti_5O_{12}$ spinel. *J. Am. Chem. Soc.* **131**, 17786 (2009).
13. A. Guerfi: Nano-particle $Li_4Ti_5O_{12}$ spinel as electrode for electrochemical generators. *J. Power Sources* **119–121**, 88 (2003).
14. M. Hirayama, K. Kim, T. Toujigamori, W. Cho, and R. Kanno: Epitaxial growth and electrochemical properties of $Li_4Ti_5O_{12}$ thin-film lithium battery anodes. *Dalton Trans.* **40**, 2882 (2011).
15. M. Hirayama, H. Ido, K. Kim, W. Cho, K. Tamura, J.i. Mizuki, and R. Kanno: Dynamic structural changes at $LiMn_2O_4$/electrolyte interface during lithium battery reaction. *J. Am. Chem. Soc.* **132**, 15268 (2010).
16. M. Hirayama, N. Sonoyama, M. Ito, M. Minoura, D. Mori, A. Yamada, K. Tamura, J. Mizuki, and R. Kanno: Characterization of electrode/electrolyte interface with x-ray reflectometry and epitaxial-film $LiMn_2O_4$ electrode. *J. Electrochem. Soc.* **154**, A1065 (2007).
17. M. Hirayama, N. Sonoyama, T. Abe, M. Minoura, M. Ito, D. Mori, A. Yamada, R. Kanno, T. Terashima, M. Takano, K. Tamura, and J. Mizuki: Characterization of electrode/electrolyte interface for lithium batteries using in situ synchrotron x-ray reflectometry—A new experimental technique for $LiCoO_2$ model electrode. *J. Power Sources* **168**, 493 (2007).
18. H. Bryngelsson, M. Stjerndahl, T. Gustafsson, and K. Edström: How dynamic is the SEI? *J. Power Sources* **174**, 970 (2007).
19. M. Herstedt, A.M. Andersson, H. Rensmo, H. Siegbahn, and K. Edström: Characterisation of the SEI formed on natural graphite in PC-based electrolytes. *Electrochim. Acta* **49**, 4939 (2004).
20. T. Eriksson, A.M. Andersson, A.G. Bishop, C. Gejke, T. Gustafsson, and J.O. Thomas: Surface analysis of $LiMn_2O_4$ electrodes in carbonate-based electrolytes. *J. Electrochem. Soc.* **149**, A69 (2002).
21. J. Liu, P. Bian, J. Li, W. Ji, H. Hao, and A. Yu: Gassing behavior of lithium titanate based lithium ion batteries with different types of electrolytes. *J. Power Sources* **286**, 380 (2015).
22. M. He, E. Castel, A. Laumann, G. Nuspl, P. Novak, and E.J. Berg: In situ gas analysis of $Li_4Ti_5O_{12}$ based electrodes at elevated temperatures. *J. Electrochem. Soc.* **162**, A870 (2015).
23. M-S. Song, R-H. Kim, S-W. Baek, K-S. Lee, K. Park, and A. Benayad: Is a solid-electrolyte-interphase-free electrode material in Li-ion batteries? Reactivity between the $Li_4Ti_5O_{12}$ electrode and electrolyte. *J. Mater. Chem. A* **2**, 631 (2014).
24. Y-B. He, M. Liu, Z-D. Huang, B. Zhang, Y. Yu, B. Li, F. Kang, and J-K. Kim: Effect of solid electrolyte interface (SEI) film on cyclic performance of $Li_4Ti_5O_{12}$ anodes for Li ion batteries. *J. Power Sources* **239**, 269 (2013).
25. X. Lu, L. Gu, Y-S. Hu, H-C. Chiu, H. Li, G.P. Demopoulos, and L. Chen: New insight into the atomic-scale bulk and surface structure evolution of $Li_4Ti_5O_{12}$ anode. *J. Am. Chem. Soc.* **137**, 1581 (2015).
26. M. Kitta, T. Akita, and M. Kohyama: Spontaneous Li-ion transfer from spinel $Li_4Ti_5O_{12}$ surfaces: Deterioration at $Li_4Ti_5O_{12}$/electrolyte interfaces stored at room temperature. *J. Electrochem. Soc.* **162**, A1272 (2015).
27. M. Kitta, T. Akita, Y. Maeda, and M. Kohyama: Study of surface reaction of spinel $Li_4Ti_5O_{12}$ during the first lithium insertion and extraction processes using atomic force microscopy and analytical transmission electron microscopy. *Langmuir* **28**, 12384 (2012).
28. K. Kim, T. Toujigamori, K. Suzuki, S. Taminato, K. Tamura, J. Mizuki, M. Hirayama, and R. Kanno: Characterization of nano-sized epitaxial $Li_4Ti_5O_{12}$(110) film electrode for lithium batteries. *Electrochemistry* **80**, 800 (2012).
29. C.F. Majkrzak: Applications of specular neutron reflectometry in materials science. *J. Neutron Res.* **7**, 159 (1999).
30. M. Yonemura, M. Hirayama, K. Suzuki, R. Kanno, N. Torikai, and N.L. Yamada: Development of spectroelectrochemical cells for in situ neutron reflectometry. *J. Phys.: Conf. Ser.* **502**, 012054 (2014).
31. L.G. Parratt: Surface studies of solids by total reflection of x-rays. *Phys. Rev.* **95**, 359 (1954).
32. A. Nelson: Co-refinement of multiple contrast neutron/x-ray reflectivity data using MOTOFIT. *J. Appl. Crystallogr.* **39**, 273 (2006).
33. L. Parratt: Surface studies of solids by total reflection of X-rays. *Phys. Rev.* **95**, 359 (1954).
34. N.L. Yamada, N. Torikai, K. Mitamura, H. Sagehashi, S. Sato, H. Seto, T. Sugita, S. Goko, M. Furusaka, T. Oda, M. Hino, T. Fujiwara, H. Takahashi, and A. Takahara: Design and performance of horizontal-type neutron reflectometer SOFIA at J-PARC/MLF. *Eur. Phys. J. Plus* **126**, 1 (2011).
35. K. Mitamura, N.L. Yamada, H. Sagehashi, N. Torikai, H. Arita, M. Terada, M. Kobayashi, S. Sato, H. Seto, S. Goko, M. Furusaka, T. Oda, M. Hino, H. Jinnai, and A. Takahara: Novel neutron reflectometer SOFIA at J-PARC/MLF for in-situ soft-interface characterization. *Polym. J.* **45**, 100 (2013).
36. M. Hirayama, M. Yonemura, K. Suzuki, N. Torikai, H. Smith, E. Watkinsand, J. Majewski, and R. Kanno: Surface characterization of $LiFePO_4$ epitaxial thin films by x-ray/neutron reflectometry. *Electrochemistry* **78**, 413 (2010).
37. T. Ohzuku, A. Ueda, and N. Yamamoto: Zero-strain insertion material of $Li[Li_{1/3}Ti_{5/3}]O_4$ for rechargeable lithium cells. *J. Electrochem. Soc.* **142**, 1431 (1995).

Supplementary Material

To view supplementary material for this article, please visit http://dx.doi.org/10.1557/jmr.2016.320.

https://doi.org/10.1557/jmr.2016.320 Published online by Cambridge University Press